

Simulation Study of CZTS/CZTSe Tandem Solar Cell by Using SCAPS-1D Software

Leila Ghalmi^{1,*}, Souhila Bensmaine¹, Mourad Elbar², Slimane Chala^{2,3,†}, Hayat Merzouk¹

¹ *Materials and Renewable Energy Research Unit, Faculty of Sciences, Abou Bekr Belkaid University, 13000 Tlemcen, Algeria*

² *Laboratory of Metallic and Semiconducting Materials, Mohamed Khider University, 07000 Biskra, Algeria*

³ *Institute of Electrical and Electronic Engineering, M'Hamed Bougara University, 35000 Boumerdes, Algeria*

(Received 06 October 2022; revised manuscript received 26 December 2022; published online 27 December 2022)

The solar spectrum can be divided by tandem solar cells into several subcells that have different bandgaps which convert, more effectively, the light into electricity than the single cells. In this study, the simulation of the photovoltaic (PV) characteristics of a CZTS/CZTSe tandem solar cell, based on structures of copper zinc tin sulfide (CZTS) as a top cell and copper zinc tin selenide (CZTSe) as a bottom cell, was accomplished by using SCAPS-1D simulator under AM1.5 illumination. Initially, the simulation of single CZTS and CZTSe solar cells was performed to give efficiency of 14.37 % and 17.87 %, respectively, which are in good agreement with the literature results. Before feeding with filtered spectrum, the simulated PV parameters of the CZTS/CZTSe tandem solar cell are the conversion efficiency (η) of 20.68 % and the short-circuit current density (J_{sc}) of 20.205 mA/cm² of the top and bottom cells with arbitrary normal thicknesses. Furthermore, and in order to reach the matching current, both top and bottom cells have been investigated at different thicknesses for tandem configuration after validation, where the performance of the top and bottom cells is at thicknesses ranged from 0.05-0.5 μ m and 0.1-1 μ m, respectively. The performance of the tandem solar cell is determined after filtered spectrum feeding and current matching. The J_{sc} of CZTS/CZTSe tandem solar cell is 20.33 mA/cm² for 0.255 μ m thick of the top, CZTS, cell and 0.8 μ m of the bottom, CZTSe, cell. The maximum η of 22.98 % is reached for tandem structure design with open circuit voltage (V_{oc}) enhancing of 1.48 V.

Keywords: Simulation, SCAPS-1D, CZTS/CZTSe tandem solar cell, Current matching, Filtered spectrum.

DOI: [10.21272/jnep.14\(6\).06033](https://doi.org/10.21272/jnep.14(6).06033)

PACS numbers: 78.20.Bh, 73.40.Lq, 84.60.Jt

1. INTRODUCTION

Photovoltaic (PV) thin film solar cells have attracted great deal of attention for several decades of research because of their ability to produce low cost and high efficiency with large-area thin-film solar cells [1]. The two main reasons for choosing a material as an absorber layer, based on the mechanism of the solar cell, are (1) the highlight absorption capability to excite electrons to higher states of energy and (2) the ability to move these excited electrons from the solar cell to an external circuit. Besides, as an important point, choosing non-toxic, environmentally friendly, and air-stable materials plays a crucial role in manufacturing thin film solar cells [2].

Thin film solar cells have large-scale PV applications due to their low cost of fabrication. Several semiconductor materials, such as zinc oxide (ZnO), indium tin oxide (ITO), cadmium oxide (CdO), zinc sulfide (ZnS), cadmium sulfide (CdS), polycrystalline cadmium telluride (CdTe), copper indium gallium diselenide CuInGaSe₂ (CIGS), copper zinc tin sulfide Cu₂ZnSnS₄ (CZTS), copper zinc tin selenide Cu₂ZnSnSe₄ (CZTSe) and copper zinc tin sulfur selenide Cu₂ZnSnSe₄ (CZTSSe) have been widely used in many optoelectronic applications such as photodiodes and solar cells [3-11].

The most widely used Si-based solar cell exhibits high conversion efficiency (up to 24.5 % at the University of New South Wales). However, it suffers from low throughput and high cost, therefore, cannot affect the

world's energy market [12, 13]. On the other hand, CIGS and CdTe offer high efficiencies (around 23.35 % and 21 %, respectively), for which they attracted the researchers for the last few years [14]. The PV technologies of thin films which include CdTe and CIGS rely on elements that are toxic, such as cadmium (Cd) and rare earth such as tellurium (Te), indium (In) and gallium (Ga), which makes their production limited [15, 16]. Quaternary semiconductors, CZTS, CZTSe and CZTSSe, as alternative absorber materials, have got attention with better advantages over CdTe and CIGS [17, 18]. They have different crystal structures, stannite and kesterite, where the last one shows more stability than the first one [13]. In addition, kesterites are used as a *p*-type absorber layer in solar cells [19], high absorption coefficients exceed 10⁴ cm⁻¹ [20]. One important advantage of CZTS is that it consists of earth abundant materials which are non-toxic [13]. CZTS, CZTSe and CZTSSe can be fabricated using different processes such as sputtering, evaporation, spray pyrolysis, electrodeposition, sol-gel technique, etc. [16, 21].

Recently, many studies have been performed to improve the efficiency of the solar cell based on CZTS absorber layer [22]. The best kesterite cell efficiency reported till date is 12.6 % for sulfoselenide (CZTSSe) based absorber with single CdS as a double buffer layer and 12.7 % with double CdS/In₂S₃ as an *n*-type buffer layer, respectively [23-25]. As for pure selenide, CZTSe, and pure sulfide, CZTS, the maximum efficiency is about 11.6 % and 11.01 %, respectively [26]. Using a

* leila.ghalmi@univ-tlemcen.dz

† s.chala@univ-boumerdes.dz

solar cell capacitance simulator (SCAPS), a comparative study of thin film solar cells was accomplished, where we used ZnO as a window layer, CdS as a buffer layer and CZTS, CZTSe and CZTSSe as absorber layers [1]. The limitation of light absorption by the absorber layer bandgap (E_g) is one of the main problems with single junction solar cells, i.e., photons that have energies less than E_g are not absorbed, while the excess energy of photons with energies higher than E_g is wasted as thermalization losses. In both cases, photons do not contribute to the useful output of the device [27]. Multijunction and tandem solar cells are effective solutions to this problem [28]. The CZTSSe bandgap can be changed from 1.0 eV (pure CZTSe) to 1.5 eV (pure CZTS) by altering the ratio of selenium and sulfur S/(S + Se) [17, 18, 29]. CZTSSe is, therefore, a prime candidate for application in multijunction solar cells. Because multijunction solar cells have layers with different bandgap energies which exploit different energy regions of the solar spectrum, an increase in the efficiency is expected [7]. The tandem solar cell structures utilize stacking of different band gap p - n junction solar cells in a specific configuration, where the short wavelength (high energy) part of the solar spectrum should be absorbed by the top cell; meanwhile, the bottom cell with low bandgap absorbs the rest [7].

A theoretical study of tandem CZTSSe junction solar cells has been reported with maximum efficiency of 21.7 % [8]. Also, a CZTGS/CZTS tandem cell structure has been developed and an efficiency of 17.51 % has been exhibited, which is an improvement compared to that of CZTS single cell structure [30]. In 2017, a CZTS/CZTSe tandem structure was proposed where ITO is considered as a tunnel junction between the two subcells. In order to study the tandem structure design, both top and bottom cells have been studied numerically many times and then the principles of series circuit have been used for both cell parameters. The achieved efficiency of their design was 19.87 % [28]. Furthermore, a research study of other CZTS/CZTSe tandem structure has been done and an efficiency of 21.7 % has been achieved for matched current at 211.33 nm thick CZTS top cell in conjunction with 2000 nm bottom cell [8].

In this work, we have considered a tandem structure using CZTS/CZTSe based absorber materials. The 1D electrical solar cell simulation program SCAPS-1D was used to simulate the device performances [31, 32]. Parameters of materials required for simulation studies are rationally suggested, cited or borrowed from the literature for better performance comprehending under realistic situations. In the first step, we will report the modeling and simulation results of single CZTS and CZTSe solar cells and compare them with related and previously reported simulation. In the second step, the study will be expanded for tandem solar cell structures to achieve improved photoconversion efficiencies, where we will show the simulation results of the tandem CZTS/CZTSe solar cell with CZTS as top cell absorber and CZTSe as bottom cell absorber. The matching current is the prerequisite condition in the tandem structure design for optimization the performance of the CZTS/CZTSe tandem solar cell at maximum efficiency, the same current (current matching) has been achieved with variation in the absorber layer thickness of the top

and bottom cells with filtered spectrum to enable them to have the same current density (J_{sc}). The current matching role in the improvement of the performance of the CZTS/CZTSe tandem solar cell was simulated and analyzed.

2. PRINCIPLE OF THE TANDEM SOLAR CELL

The principle of the tandem cell is shown in Fig. 1. In a tandem solar cell, top and bottom cells are electrically in series. We use the following notations.

J_{sc} tandem, V_{oc} tandem: short circuit current density and open circuit voltage of the tandem solar cell.

J_{sc} top, V_{oc} top: short circuit current density and open circuit voltage of the top cell.

J_{sc} bottom, V_{oc} bottom: short circuit current density and open circuit voltage of the bottom cell.

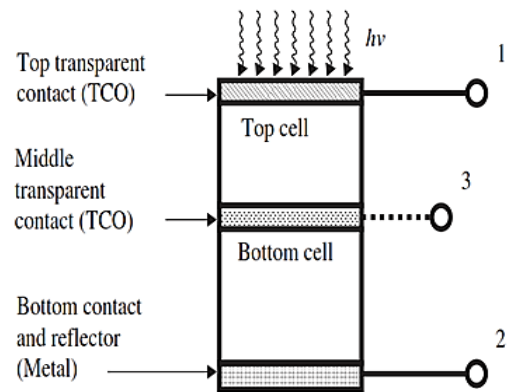


Fig. 1 – The principle of a tandem solar cell

There is a difference between J_{sc} top and J_{sc} bottom, the short circuit current density of the tandem solar cell will be given by the smaller value of the two short circuit current densities of the top and bottom cells [27, 33, 34]:

$$J_{sc} \text{ tandem} \approx \text{Min}\{ J_{sc} \text{ top}, J_{sc} \text{ bottom}\}. \quad (1)$$

The open circuit voltage of the tandem solar cell is equal to the sum of the open circuit voltages of the two top and bottom cells [27, 34]:

$$V_{oc} \text{ tandem} \approx V_{oc} \text{ top} + V_{oc} \text{ bottom}. \quad (2)$$

In the case of the condition of equal currents for optimal performance we have:

$$V_{oc} \text{ tandem} = V_{oc} \text{ top} = V_{oc} \text{ bottom}. \quad (3)$$

In the case of equal currents, the fill factor (FF) of the tandem solar cell can be considered between the FF of the top and bottom cells. However, in the case of unequal currents, the FF of the tandem solar cell is very often higher [7].

The construction of the $J(V)$ diagram of the solar cell is shown in Fig. 2.

3. THE SOLAR CELL STRUCTURE DETAILS AND NUMERICAL SIMULATION

Single junction solar cell performance is limited by the photon absorption for the respective band gap of the absorber layer of the cell. By stacking single junction

solar cells which contain absorber layers with different bandgap energies, the performance can be improved. Photons with higher and lower energies are absorbed in the top and bottom cells, respectively, that contributes to the minimization of thermalization effects [35]. In CZTS/CZTSe tandem solar cell, as shown in Fig. 3b, where the top cell has CZTS as an absorber layer with bandgap, $E_g = 1.5$ eV, and the bottom cell has CZTSe as an absorber layer with bandgap less than that in the top cell, $E_g = 1.1$ eV.

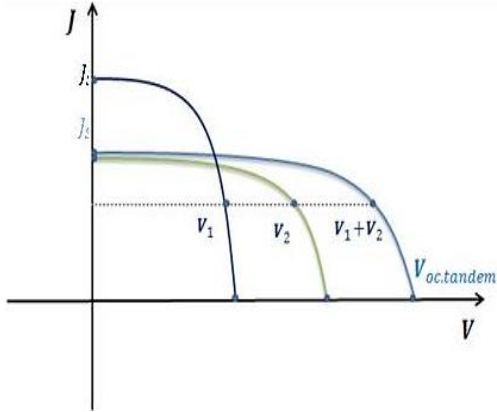


Fig. 2 – The construction of the $J(V)$ diagram characterization of a tandem solar cell [32]

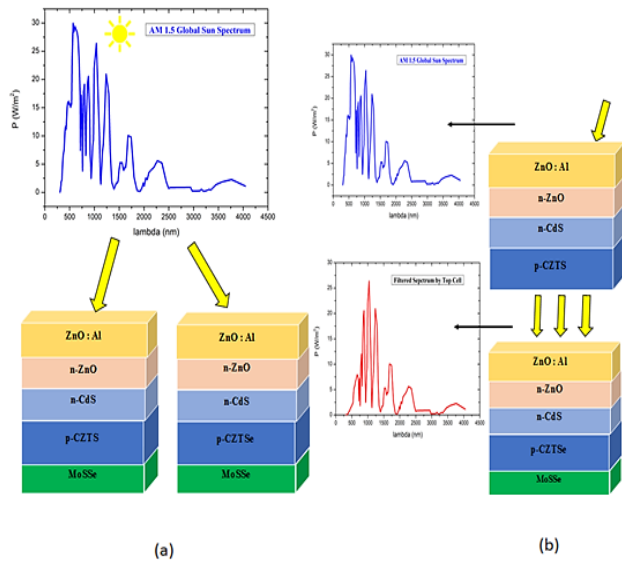


Fig. 3 – Diagram of the structure of the apparatus and illuminated spectrum of (a) CZTS(Se) based solar cell with 1.1 eV band gap, 1.5 eV in autonomous condition with AM1.5 solar spectrum, (b) tandem configuration of CZTS/CZTSe

This design is intended to convert a wide range of incident photons on the solar cell and generate maximum output power. In details, this tandem solar cell consists of a top n -CdS/ p -CZTS heterojunction solar cell and a bottom n -CdS/ p -CZTSe heterojunction solar cell, that are optically and electrically connected through a layer of aluminum doped zinc oxide (Al:ZnO) serving as a transparent conductive oxide (TCO). The tandem cell was considered to be illuminated under an AM1.5 solar

spectrum, where the incident power density is 1000 W/m^2 . It has been assumed that solar radiation is normally incident on the Al:ZnO layer which represents the front cathode contact, the rear anode contact is represented by a layer of molybdenum sulfide selenide (MoSSe). The doping concentrations and the different thicknesses used in the simulation are summarized in the Tables (1, 2).

For the numerical simulation of solar cells, we used the optoelectrical device simulator SCAPS (a solar cell capacitance simulator)-1D, developed at the Department of Electronics and Information Systems (ELIS) of the University of Ghent (Belgium) [31]. SCAPS is designed to simulate the electrical characteristics as well as the spectral response of thin film heterojunction solar cells [37, 38]. It solves a set of fundamental equations including the Poisson's equation, the continuity equations, and the charge transport equations. Poisson's equation links together the electrostatic potential and the local charge densities. Meanwhile, the continuity and transport equations describe the way that the electron and hole densities evolve as a result of generation, recombination and transport processes [31, 32, 36] and are listed in Table 3.

A detailed description of the filtered spectrum and current matching technique is discussed in the results section. The optimized parameters of material properties used to simulate the PV response of the considered single and tandem solar cells are taken from the literature [4, 20, 38, 39] and listed in Table 1 and Table 2, whereas the optical absorption spectra for CZTS and CZTSe are taken from literature [40] and for CdS and ZnO the absorption spectrum files [8], as provided in SCAPS and shown in Fig. 4. These absorption data are used to mimic the practical absorbing properties.

CZTSSe solar cells are very interesting because their parameters can be modified by changing the composition of the absorber material [20, 41]. The electron mobility (μ_p), hole mobility (μ_n), the effective density of states of the conduction band (N_c), and the effective density of states of the valence band (N_v) have been defined for each layer [19]. In our simulation, we have chosen a value of 4.2 eV for the electron affinity of the CZTSSe material and the operating temperature was set at 300 K.

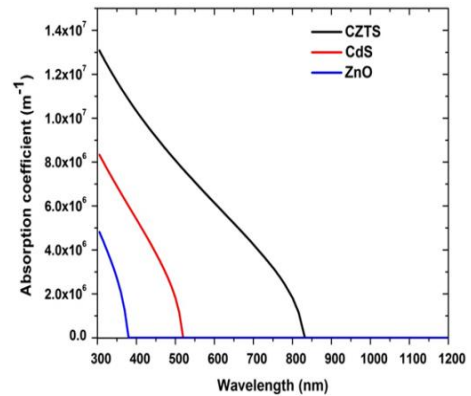


Fig. 4 – The absorption coefficients of different materials used in the present work

Table 1 – Parameters set for the simulation of the CZTS, CZTSe based solar cells, A and D denote acceptor and donor defects

Layer properties	ZnO: Al	ZnO	CdS	CZTSe	CZTS	MoSSe
Thickness (nm)	300	50	50	variable	variable	350
Electron affinity χ_e (eV)	4.40	4.40	4.20	1.1	1.5	4.140
Layer band gap E_g (eV)	3.30	3.30	2.40	4.2	4.2	1.10
Relative permittivity ϵ_r (F·cm ⁻¹)	9	9	10	10	10	13.60
Conduction band effective density of states N_c (cm ⁻³)	10 ¹⁸	10 ¹⁸	10 ¹⁸	2.2 × 10 ¹⁸	2.210 × 10 ¹⁸	2.20 × 10 ¹⁸
Valence band effective density of states N_v (cm ⁻³)	10 ¹⁹	10 ¹⁹	10 ¹⁹	1.8 × 10 ¹⁹	1.8 × 10 ¹⁹	1.80 × 10 ¹⁹
Electron mobility μ_n (cm ² /V·s)	10 ²	10 ²	10 ²	10 ²	10 ²	10 ²
Hole mobility μ_p (cm ² /V·s)	25	25	25	25	25	25
Donor concentration N_D (cm ⁻³)	10 ¹⁸	10 ¹⁷	10 ¹⁸	0	0	0
Acceptor concentration N_A (cm ⁻³)	0	0	0	3.0 × 10 ¹⁷	10 ¹⁷	10 ¹⁶
Absorption coefficient (cm ⁻¹ Ev ^{1/2})	SCAPS	SCAPS	SCAPS	Data file	Data file	Data file

Table 2 – Simulation parameters of defect states densities and electron (hole) capture cross-sections

Parameters and units	ZnO: Al	ZnO	CdS	CZTSe	CZTS	MoSSe
Defect type	Single Donor (0/+)	Single Donor (0/+)	Single Acceptor (-/0)	(A)/(D)	(A)/(D)	Single Donor (0/+)
Capture cross section electrons (cm ²)	5.0 × 10 ⁻¹³	5.0 × 10 ⁻¹⁵	10 ⁻¹³	3 × 10 ⁻¹⁴ /10 ⁻¹⁵	3 × 10 ⁻¹⁴ /10 ⁻¹⁵	10 ⁻¹³
Capture cross section holes (cm ²)	10 ⁻¹⁵	10 ⁻¹³	10 ⁻¹⁵	10 ⁻¹⁴ /9 × 10 ⁻¹⁶	10 ⁻¹⁴ /9 × 10 ⁻¹⁶	10 ⁻¹⁵
Energetic distribution	Single	Single	Single	Single	Single	Single
Reference for defect energy level E_t	Above E_V	Above E_V	Above E_V	Above E_V	Above E_V	Above E_V
Peak energy position E_{GA} , E_{GD} (eV)	1.650	1.650	1.20	0.2, 0.7	0.2, 0.85	0.8
Deep defect density (cm ⁻³)	1.8 × 10 ¹⁶	5.0 × 10 ¹⁴	6.0 × 10 ¹⁷	9.80×10 ⁺¹⁵ 8.0×10 ⁺¹⁶	9.80 × 10 ¹⁵ 8.0 × 10 ¹⁶	4.0 × 10 ¹⁴

Table 3 – The fundamental equations were used during the SCAPS 1D, simulation transmitted spectrum and computing efficiency [29, 30, 39, 46]

Gaussian Defect	<p>Range,</p> $[E_t - \frac{W_G}{2} E_c ; E_t + \frac{W_G}{2} E_c]$ $E_t(E) = N_{peak} \times \exp\left[-\left(\frac{E - E_t}{E_c}\right)^2\right]$ $N_{tot}(N_{peak}) = E_c E_{peak}$ <p>where E_t is the energy level of the trap, E_c is the characteristic energy, W_G is the width of the Gaussian energy distribution (default 6.0 is used), N_t is the defect density in cm⁻³/eV, N_{peak} is the energy density at the peak of the distribution in cm⁻³/eV, and $N_{tot}(N_{peak})$ is the total integrated defect density on all energies cm⁻³.</p>
Optical model of SCAPS	$N_{phot}(\lambda, x) = N_{photo}(\lambda) \cdot T_{front}(\lambda) \cdot \exp(-x \cdot a(\lambda)) \times \left(\frac{1 + R_{back}(\lambda) \cdot \exp(-2(d-x) \cdot a(\lambda))}{1 - R_{back}(\lambda) \cdot R_{int}(\lambda) \exp(-2d \cdot a(\lambda))}\right)$ $E_t(E) = N_{peak} \times \exp\left[-\left(\frac{E - E_t}{E_c}\right)^2\right]$ $N_{tot}(N_{peak}) = E_c E_{peak}$ <p>where, $N_{phot}(\lambda, x)$ is the photon flux at each position of the layer, $N_{photo}(\lambda)$ is the incident photon flux, $T_{front}(\lambda)$ is the front contact transmission, $a(\lambda)$ is the coefficient of absorption, R_{int} is the internal reflection at the front contact (the default value 0 is used), $R_{back}(\lambda)$ is the reflection at the rear contact (the default value 0 is used), d is the thickness of the layer, x is the position in the shell, and $G(x)$ is the rate of generation of electron-hole pairs. This model only includes two contact reflections / transmissions and absorption in the semiconductor layer. It does not integrate scattering, interference and intermediate reflections.</p>
One-dimensional equations of semi-conductors.	$\frac{\partial}{\partial x} \left(\epsilon_0 \epsilon \frac{\partial \Psi}{\partial x} \right) = q(p - n + N_D^+ - N_A^- + p_t - n_t)$ $\frac{\partial}{\partial x} \left(\epsilon_0 \epsilon \frac{\partial \Psi}{\partial x} \right) = q(p - n + N_D^+ - N_A^- + p_t - n_t)$ $-\frac{\partial J_n}{\partial x} - U_n + G = \frac{\partial n}{\partial t}$ $-\frac{\partial J_p}{\partial x} - U_p + G = \frac{\partial p}{\partial t}$

	$J_n = -\frac{\mu_n n \partial E_{Fn}}{q \partial x}$ $J_p = +\frac{\mu_p p \partial E_{Fp}}{q \partial x}$ <p>where q is the electronic charge, Ψ is the electrostatic potential, p, n, p_i, n_i are respectively the free hole, the free electron, the trapped hole and the trapped electron. N_D^+, N_A^- is respectively the doping concentration of ionized donor type and the doping concentration of ionized acceptor type. E is the permittivity and ϵ_0 is the permittivity of free space, J_n is the current density of electrons, J_p is the current density of holes, U_n is the rate of recombination of electrons, U_p is the rate of recombination of holes, G is the generation rate, μ_n is the electron mobility, μ_p is the mobility of the hole, E_{Fn} is the quasi-Fermi level of electrons, and E_{Fp} is the quasi-Fermi hole.</p>
Spectrum transmitted by top cell	$S(\lambda) = S_0(\lambda) \cdot \exp\left(\sum_{i=1}^3 - (a_{material_i}(\lambda) \cdot d_{material_i})\right)$ $S(\lambda) = S_0(\lambda) \cdot (\exp(-\alpha_{ZnO}(\lambda) \cdot d_{ZnO}) \cdot \exp(-\alpha_{CdS}(\lambda) \cdot d_{CdS}) \cdot \exp(-\alpha_{ZnO}(\lambda) \cdot d_{ZnO}) \cdot \exp(-\alpha_{CZTS}(\lambda) \cdot d_{CZTS}))$ <p>here, $S_0(\lambda)$ is the incident spectrum AM1.5G, a_i and d_i are the absorption coefficient, and d represents the thickness of the respective layer. Losses by interfacial reflection are ignored. In addition, material1, material2 and material3 refer to ZnO, CdS, CZTS, respectively.</p>
FF and efficiency of solar cell	$FF = \frac{V_{max} \times I_{max}}{V_{oc} \times I_{sc}}, \eta = \frac{V_{oc} \times I_{sc} \times FF \times 100}{P_{in}}$ <p>The optimal point between $V = 0$ and $V = V_{oc}$ is V_{max}, whereas I_{max} relates with V_{max}</p>

4. RESULTS AND DISCUSSION

4.1 Modeling of CZTSe and CZTS Single Solar Cells

The single junction solar cell structures are shown in Fig. 3a: Al:ZnO/ZnO/ n -CdS/ p -absorber layer/MoSSe, where the p -absorber layer is whether CZTS or CZTSe materials, n -CdS is a wide band gap buffer layer, ZnO is a window layer, as well as a passivation layer, Al:ZnO is a TCO layer and MoSSe is a back contact layer. The material properties are summarized in Table 1 and Table 2, used to simulate the PV response for the proposed single and tandem device structures.

4.2 Impact of the Absorber Layer, CZTS or CZTSe, Thickness on Single Junction PV Performance

In order to summarize the performance of both devices with different thicknesses, the PV parameters are quantified and plotted in Fig. 5a-h. V_{oc} , J_{sc} , FF and the efficiency (η) for the top cell are reported in Fig. 5a-d, whereas for the bottom cell, the same parameters are depicted in Fig. 5e-h. The results show that FF of the CZTS solar cell decreases with increasing CZTS layer thickness from 0.05 to 0.25 μm and saturates with further increase. Meanwhile, the FF of the CZTSe solar cell increases with increasing CZTSe layer thickness from 0.1 to 0.4 μm and saturates with further increase. Higher thickness increases the series resistance and recombination rate, both these factors are responsible for lowering the FF [42]. J_{sc} of the CZTS solar cell shows a significant increase with increasing the CZTS layer thickness from 0.05 to 0.25 μm and saturates with further increase, while, in the CZTSe solar cell, J_{sc} shows a small increase with increasing the CZTSe layer thickness from 0.1 to 0.4 μm and saturates with further increase. We found that the CZTS solar cell exhibits relatively large V_{oc} , Fig. 5c, as compared to that of the CZTSe solar cell Fig. 5g. Although, a slight increase in V_{oc} for the CZTS solar cell with increasing CZTS thickness is noticed, approaching the optimal V_{oc} , there is no significant effect of the thickness of both solar cell absorbers. The high V_{oc} of the CZTS

solar cell is mainly due to its larger bandgap compared to the CZTSSe solar cell [27]. By increasing the CZTS layer thickness from 0.05 to 0.255 μm for the CZTS cell and the CZTSe layer thickness from 0.1 to 0.4 μm for the CZTSe cell, the conversion efficiency of the CZTS and CZTSe solar cells is augmented from 5.8 to 14.37 % and from 15.71 to 17.87 %, respectively, showing the saturation after a critical thickness. Clearly, the thickness of 0.25 μm and 0.4 μm is sufficient to achieve the maximum PV response for CZTS and CZTSe solar cells, respectively.

The simulation results of $J(V)$ characteristics for single CZTS and CZTSe solar cells are shown in Fig. 6, and their PV parameters extracted from the corresponding $J(V)$ curves are given in Table 4. Clearly, our results of simulation are in good agreement with the results in [8], thus the parameters and model used in the simulation are suitable and validate.

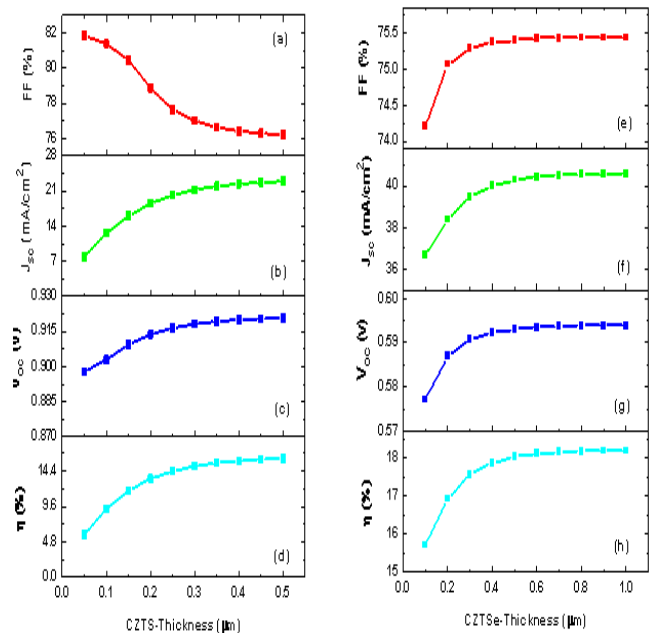
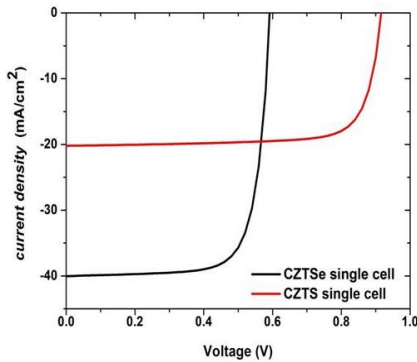


Fig. 5 – PV parameter of single (a-d) CZTS and (e-h) CZTSe solar cells with different absorber layer thicknesses

Table 4 – Comparison of the photovoltaic parameter of single CZTS and CZTSe solar cell with other single structures from the literature

Structure	J_{sc} (mA/cm ²)	V_{oc} (V)	FF (%)	η (%)	Refs
CZTS single cell (255 nm)	20.205	9.165	77.62	14.37	Present work
CZTS single cell (211nm)	20.98	0.852	81.95	14.67	[8]
CZTSe single cell (400 nm)	40.02	5.924	75.37	17.87	Present work
CZTSe single cell (2000 nm)	20.98	0.852	81.95	14.67	[8]

**Fig. 6** – $J(V)$ characteristics of single CZTSe and CZTS solar cells

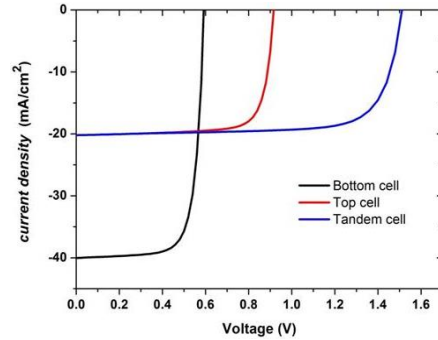
4.3 Modeling the Tandem Solar Cell in CZTS/CZTSe

The structure of the CZTS/CZTSe tandem solar cell is shown in Fig. 3b and the simulation parameters are indicated in Table 1 and Table 2. The top CZTS and bottom CZTSe cells are optically and electrically connected with a transparent conductive oxide layer of Al:ZnO. To model the transparent ZnO interconnect layer in the tandem cell, one approach is used and is to add an electrode that exactly covers the transparent ZnO interconnect layer and attach a localized resistance to it using the statement in SCAPS-1D [31]. By doing this, we are forcing the current to flow from the anode to the cathode and preventing any current from flowing through the extra electrode. Physically, this can be justified by the fact that the interconnect layer acts as a resistor allowing current to flow without significant limitation. The resistance value can be used to adjust the amount of current to flow through the additional electrode, which helps control the resistance of the intermediate layer [6, 42].

The electrical characteristic $J(V)$ of the CZTS/CZTSe tandem solar cell before optimization, under illumination by the 1.5 AM solar spectrum with a power density of 100 mW/cm² is shown in Fig. 7.

To obtain the $J(V)$ curves of the top and bottom cells, the anode and cathode contacts of the top, CZTS, cell were placed at the interconnect Al:ZnO layer and the top Al:ZnO layer, respectively, while the anode and

cathode contacts of the bottom, CZTSe, cell were placed at the back MoS₂ layer and the interconnect Al:ZnO layer, respectively. It is observed from Fig. 7 that the J_{sc} of the tandem solar cell is limited by the lower J_{sc} of the top, CZTS, cell because the top and bottom cells were current mismatched [30]. The tandem J_{sc} value of 20.205 mA/cm² is approximately equal to the top cell J_{sc} value of 20.21 mA/cm², while the V_{oc} value of the tandem cell, $V_{oc} = 1.51$ V, is equal to the sum of the top cell, $V_{oc} = 0.92$ V, and that of the bottom cell, $V_{oc} = 0.59$ V. From these results, the proper functioning of the CZTS and CZTSe cells connected in series forming the tandem solar cell is demonstrated. Moreover, the FF of the tandem cell, 67.36 %, is relatively lower than that of the top cell, 77.62 %, and that of the bottom cell, 75.37 %. Although there is a decrease in the FF, the increase in the V_{oc} of the tandem cell led to an improvement in its efficiency, $\eta = 20.68$ %, compared to that of CZTS (top) cell, $\eta = 14.37$ %, and CZTSe (bottom) cell, $\eta = 17.87$ %.

**Fig. 7** – $J(V)$ characteristics of the CZTS top cell, CZTSe bottom cell and CZTS/CZTSe tandem cell before fed with filtered spectrum

4.4 Filtered Spectrum and Matching Current the Tandem Solar Cell

This section is dedicated to the comprehensive study of the CZTS/CZTSe tandem solar cell by employing the top and bottom cells discussed in previous sections. The AM1.5 spectrum, as shown in Fig. 3a, is illuminated to the top cell and the transmitted spectrum, $S(\lambda)$, by the top cell is calculated with the help of the absorption coefficient and thickness of all the layers used in the top cell as stated in Table 3. Whereas the bottom cell is exposed to the filtered spectra calculated by using the transfer matrix method at various absorber layer thicknesses in the top cell [44]. Initially, the top cell is simulated by varying the absorber layer thickness from 50 to 500 nm (to get eleven filtered spectra), while doing so, the thickness of the rest layers is kept constant. The filtered transmitted spectrum by the top cell with various absorber layer thicknesses is illustrated in Fig. 8.

Increasing the thickness of the top cell reduces the transmission and corresponding filtered spectrum power for the wavelengths below the cutoff wavelength of both top cells, as shown in Fig. 3. This is attributed to higher absorption in the top cell with an increase in thickness, and it is worth noting that the absorber layer thickness of only 50 nm reduces the power level of standard AM1.5

spectrum from 1000 to 818.59 $\text{W}\cdot\text{m}^{-2}$ as shown in Fig. 8a. It is evident from the plots that by varying the thickness of the top cell for both solar cells from 50 to 500 nm, the number of photons transmitted by the top cell to the bottom cell decreases. Consequently, it decreases the integrated transmitted power from 818.59 to 443.89 W/m^2 by the top cell, as shown in Fig. 8b. Hence, we have augmented the thicknesses of both top and bottom cells to match the maximum deliverable J_{sc} , which is constrained by the limiting cell, i.e., top cell. To achieve the same J_{sc} , the filtered power spectrum for eleven different thicknesses of the top cell is used to conceive the presence of the top cell with different absorber layer thicknesses from 50 to 500 nm, as shown in Fig. 8a. These spectrum files are fed to the bottom cell to measure its performance. Concurrently, the thickness from 0.05 to 1 μm is to calculate all the possible thickness value points where matching current is possible. This effort resulted in the formation of the matching current, J_{sc} , curve, as shown in Fig. 9a, at various thicknesses of the top and bottom cells. Eleven intersecting points are observed for the top cell thickness ranging from 50 to 500 nm and bottom cell thickness ranging from 100 to 1000 nm. After identifying the corresponding top and bottom cell thicknesses to get matched J_{sc} from the tandem solar cell, the top cells are re-simulated with the current matched thicknesses under standard AM1.5 spectrum, and another set of filtered spectrums are constructed with considered thicknesses.

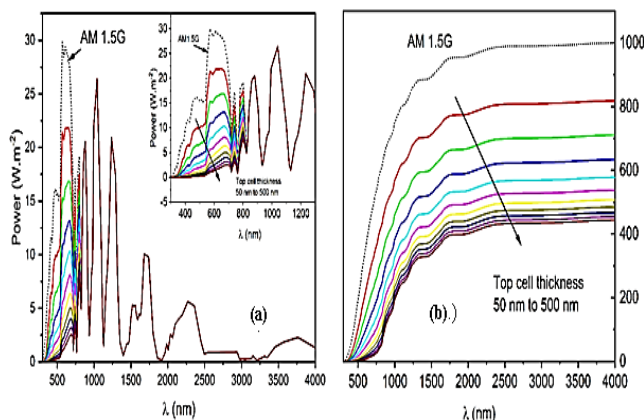


Fig. 8 – (a) Filtered spectrum by the top cell with different absorber layer (CZTS) thickness from 50 to 500 nm. The spectrum data of AM1.5 is also produced for the comparison. (b) Integrated filtered spectrum power transmitted by the top cell with different absorber layer (CZTS) thickness from 50 to 500 nm. The spectrum data of AM1.5 is also produced for the comparison

Because the absorption coefficient $\alpha(h\nu)$ for solar cell materials is not infinite, a solar cell of finite thickness will not absorb all the incident light of photon energy above the bandgap. Some light will be transmitted (especially at photon energies near the band gap where α is small) [45]. Electrically, the tandem solar cell acts as two diodes connected in series and due to this configuration, all the time equal current must pass through each cell [42, 46]. Therefore, in tandem solar cells, the thickness of both top and bottom cells is optimized to have the same J_{sc} value [42]. Under the condition of “current matching”, where the top, bottom and

tandem cells have the same J_{sc} , corresponding to maximum conversion efficiency of the tandem cell [7, 45].

This has been done using computed filtered spectrum with different absorber layer thicknesses of the top cell, as shown in Fig. 8a. To account for different top cell thickness, eleven filtered spectra, as shown in Fig. 8a, are illuminated on the bottom cell, and PV parameters of the bottom cell are evaluated. Further, for each filtered spectrum, the bottom cell thickness also varies from 50 to 500 nm in 10 equal steps. The J_{sc} values of the bottom cell under filtered spectrum are used to determine the current matching condition for the tandem solar cell, as shown in Fig. 9a. The current matched conditions for the tandem structure are obtained at the point of intersection of the top and bottom cell current densities. The best obtained matching current with the top cell thickness of 255 nm and bottom cell thickness of 800 nm, which exhibits J_{sc} values of 20.33 mA/cm^{-2} and 20.26 mA/cm^{-2} , respectively, as shown in Fig. 9a.

The V_{oc} of the top, CZTS, and bottom, CZTSe, solar cells as a function of the top, CZTS, layer thickness in a CZTS/CZTSe tandem solar cell is shown in Fig. 9b. The V_{oc} of the top cell increases with CZTS layer thickness. This is mainly because that the thicker CZTS absorber layer will absorb more photons with longer wavelength, which will, in turn, make a contribution to the generation of electron hole pairs [7]. However, the V_{oc} of the bottom cell at different thickness is nearly independent of the variation of the CZTS layer thickness.

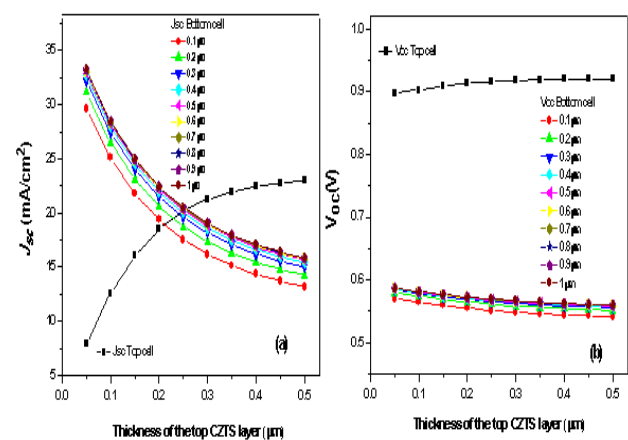


Fig. 9 – (a) Variation of the current density of the CZTS top and CZTSe bottom cells at different thicknesses and (b) open-circuit voltages of the top CZTS and bottom CZTSe solar cells as a function of the top CZTS layer thickness in a CZTS/CZTSe tandem solar cell

The matched J_{sc} values are summarized in Fig. 10a for absorber thickness of the top and bottom cells. We observed that the thickness of the top, CZTS, cell for matched tandem solar cell structure varies significantly for different bottom, CZTSe, cell thickness. This variation suggests that the current matching condition can be achieved at the relatively lower top, CZTS, cell thickness as compared to that of the bottom, CZTSe, cell thickness.

Under current matching conditions at the optimal CZTS layer thickness of 0.255 μm and CZTSe layer thickness of 0.8 μm , the $J(V)$ characteristics of the top,

bottom and tandem cells are plotted in Fig. 10b. The PV parameters at the current matching point are summarized in Table 5. The J_{sc} of the top, bottom and tandem cells are all equal to the maximum $J_{sc} = 20.33 \text{ mA/cm}^2$. The V_{oc} of the tandem cell, 1.48 V, is equal to the sum of the V_{oc} of the top cell, 0.917 V, and the bottom cell, 0.567 V. The η of the tandem solar cell, working at current matching condition and after fed with filtered spectrum, is improved to 22.91 % compared to the conversion efficiency 20.68 % obtained for the CZTS/CZTSe tandem cell working at mismatched J_{sc} and before fed with filtered spectrum. Compared to previous simulation studies, Table 6, by SCAPS-1D software, our simulated CZTS/CZTSe tandem solar cell η of 22.91 % is in good agreement with simulation results found in the literature [18, 27, 8, 47].

Table 5 – Optimized photovoltaic parameters of top, bottom and tandem solar cells under short-circuit current densities matching and after fed with filtered spectrum

Structure	J_{sc} (mA/cm ²)	V_{oc} (V)	FF (%)	η (%)
CZTS single cell (255 nm)	20.33	0.917	77.56	14.46
CZTSe single cell (800 nm)	40.55	0.594	75.48	18.17
CZTS top cell in tandem structure (255 nm)	20.33	0.917	77.56	14.46
CZTSe bottom cell (800 nm) under filtered spectrum by top (255 nm)	20.26	0.567	73.65	8.48
Tandem cell with top (255 nm) and bottom (800 nm)	20.33	1.484	75.94	22.91

Table 6 – Comparison of PV parameters of present work with other tandem structures from the literature

Structure	J_{sc} (mA/cm ²)	V_{oc} (V)	FF (%)	η (%)	Refs
CZTS/CZTSe (0.2 μm /0.85 μm)	19.17	1.43	72.60	19.86	[44]
CZTS/CTS (0.7 μm /0.8 μm)	24.85	1.41	62.04	21.77	[39]
CZTS/CZTSe (0.211 μm /2 μm)	20.98	1.32	78.20	21.7	[8]
CZTS/CZTSe (0.147 μm /3 μm)	20.4	1.1	81.30	19.25	[25]
CZTS/CZTSe (0.255 μm /0.8 μm)	20.33	1.48	75.94	22.91	Present work

5. CONCLUSIONS

Based on the SCAPS-1D simulator, we presented a numerical simulation to analyze the performance of single CZTS and CZTSe solar cells and a tandem, CZTS/CZTSe, solar cell under the AM1.5 light spectrum. The $J(V)$ characteristics and associated PV parameters were determined. We first simulated separately optimized single CZTSe and CZTS solar cells and found conversion efficiencies of about $\eta = 14.37\%$ and $\eta = 17.87\%$, respectively, which is in good agreement with simulation results. Then we studied the performance of the CZTS/CZTSe tandem solar cell with CZTS as the top cell and CZTSe as the bottom cell. An enhancement in the conversion efficiency of 20.68 % was

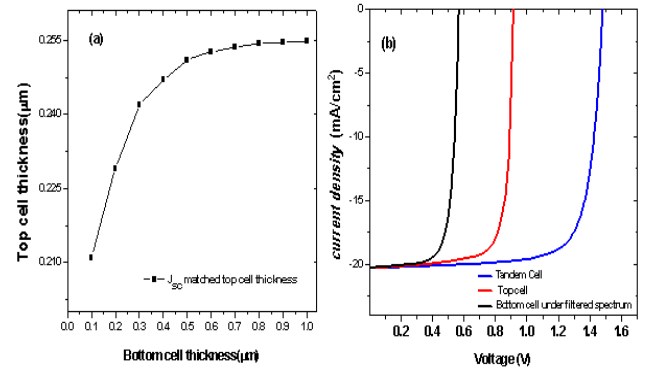


Fig. 10 – (a) Thickness of the top CZTS cell versus different thickness of the bottom CZTSe cell; (b) $J(V)$ characteristics of the CZTS top-cell, CZTSe bottom-cell and CZTS/CZTSe tandem cell under short-circuit current densities matching and after fed with filtered spectrum

achieved for the CZTS/CZTSe tandem solar cell structure with arbitrary normal thicknesses of the top and bottom cells. Lower J_{sc} limitation and V_{oc} superimposition characteristics of the series connection of the top and bottom cells were demonstrated. Finally, the top cell was illuminated with standard AM1.5 spectrum, whereas the bottom cell was analyzed under the filtered spectrum by the top cell. For realistic tandem operation, the current matching conditions were examined by varying the absorber layer thickness in both top and bottom cells. The best η of the CZTS/CZTSe tandem solar cell at 22.91 % was achieved at an optimal thickness of the CZTS layer of the top cell, 0.255 μm , and of the CZTSe layer of the bottom cell, 0.8 μm , where the bottom cell was fed with the filtered spectrum by the top cell. The condition of matching current, where the top, bottom, and tandem cells have the same short-circuit current density of 20.33 mA/cm², which is also the maximum of the tandem cell J_{sc} at an optimal thickness of the top and bottom cells, must be satisfied for the maximum η . The present study showed that a CZTS/CZTSe tandem solar cell design improved the performance of these single CZTS and CZTSe cells due to the absorption of more solar photons.

ACKNOWLEDGEMENTS

L. Ghalmi et al. would like to thank the Materials and Renewable Energy Research Unit, University of Tlemcen, and the Algerian General Directorate of Scientific Research and Technological Development (DGRSDT) for their scientific and academic support.

REFERENCES

- O.K. Simya, A. Mahaboobatcha, K. Balachander, *Superlattice Microst.* **82**, 248 (2015).
- M. Minbashi, A. Ghobadi, E. Yazdani, A. Ahmadkhan Kordbacheh, A. Hajjiah, *Sci. Rep.* **10**, 21813 (2020).
- S. Chala, R. Boumaraf, A.F. Bouhdjar, M. Bdirina, M. Labed, T.E. Taouririt, M. Elbar, N. Sengouga, F. Yakuphanoglu, S. Rahmane, Y. Naoui, Y. Benbouzid, *J. Nano-Electron. Phys.* **13** No 1, 01009 (2021).
- S. Tobbeche, S. Kalache, M. Elbar, M.N. Kateb, M.R. Serdouk, *Opt. Quantum Electron.* **51**, 284 (2019).
- M.N. Kateb, S. Tobbeche, *Opt. Quantum Electron.* **53**, 605 (2021).
- S. Chala, M. Bdirina, M. Elbar, Y. Naoui, Y. Benbouzid, T.E. Taouririt, M. Labed, R. Boumaraf, A.F. Bouhdjar, N. Sengouga, F. Yakuphanoglu, S. Rahmane, *Trans. Electr. Electron. Mater.* **23**, 544 (2022).
- M. Elbar, S. Tobbeche, A. Merazga, *Sol. Energy* **122**, 104 (2015).
- G.K. Gupta, A. Dixit, *Opt. Mater.* **82**, 11 (2018).
- Mamta, K.K. Maurya, V.N. Singh, *Coatings* **12**, 405 (2022).
- S. Chala, N. Sengouga, F. Yakuphanoglu, *Vacuum* **120**, 81 (2015).
- T.E. Taouririt, A. Meftah, N. Sengouga, M. Adaika, S. Chala, A. Meftah, *Nanoscale* **11**, 23459 (2019).
- M. Kaur, H. Singh, *Int. J. Core Eng. Manag.* **3**, 1 (2016).
- F.A. Jhuma, M.Z. Shaily, M.J. Rashid, *Mater. Renew. Sustain. Energy* **8**, 6 (2019).
- M. Green, E. Dunlop, J. Hohl-Ebinger, M. Yoshita, N. Kopidakis, X. Hao, *Prog. Photovolt. Res. Appl.* **29**, 657 (2021).
- A. Bouarissa, A. Gueddim, N. Bouarissa, H. Maghraoui-Meherezi, *Mater. Sci. Eng. B* **263**, 114816 (2021).
- M.P. Suryawanshi, G.L. Agawane, S.M. Bhosale, S.W. Shin, P.S. Patil, J.-H. Kim, A.V. Moholkar, *Mater. Technol.* **28**, 98 (2013).
- C. Zeng, Y. Liang, L. Zeng, L. Zhang, J. Zhou, P. Huang, R. Hong, *Sol. Energy Mater. Sol. C.* **203**, 110167 (2019).
- U. Saha, M.K. Alam, *RSC Adv.* **7**, 4806 (2017).
- S. Tripathi, S. Maurya, B. Kumar, D.K. Dwivedi, *IEEE 2020 International Conference on Electrical and Electronics Engineering (ICE3)*, 588 (2020).
- S. Chen, A. Walsh, X.G. Gong, S.H. Wei, *Adv. Mater.* **25**, 1522 (2013).
- D.H. Son, Y.I. Kim, S.H. Kim, D. Nam, H. Cheong, J.K. Kang, K.J. Yang, D.H. Kim, *J. Mater. Chem. A* **7**, 22986 (2019).
- H. Katagiri, K. Jimbo, W.S. Maw, K. Oishi, M. Yamazaki, H. Araki, A. Takeuchi, *Thin Solid Films* **517**, 2455 (2009).
- J. Kim, H. Hiroi, T.K. Todorov, O. Gunawan, M. Kuwahara, T. Gokmen, D. Nair, M. Hopstaken, B. Shin, Y.S. Lee, W. Wang, H. Sugimoto, D.B. Mitzi, *Adv. Mater.* **26**, 7427 (2014).
- W. Wang, M.T. Winkler, O. Gunawan, T. Gokmen, T.K. Todorov, Y. Zhu, D.B. Mitzi, *Adv. Energy Mater.* **4**, 1301465 (2014).
- R.B.V. Chalapathy, M.G. Gang, C.W. Hong, J.H. Kim, J.S. Jang, J.H. Yun, J.H. Kim, *Sol. Energy* **159**, 260 (2018).
- M.A. Green, E.D. Dunlop, D.H. Levi, J. Hohl-Ebinger, M. Yoshita, A.W.Y. Ho-Baillie, *Prog. Photovolt. Res. Appl.* **27**, 565 (2019).
- A.E. Benzetta, M. Abderrezek, M.E. Djeghlal, *Optik* **242**, 167320 (2021).
- S. Amiri, S. Dehghani, *J. Electron. Mater.* **49**, 2164 (2020).
- C. Zeng, Y. Liang, L. Zeng, L. Zhang, J. Zhou, P. Huang, R. Hong, *Sol. Energy Mater. Sol. C.* **203**, 110167 (2019).
- A.D. Adewoyin, M.A. Olopade, O.O. Oyebola, M.A. Chendo, *Optik* **176**, 132 (2019).
- M. Burgelman, P. Nollet, S. Degraeve, *Thin Solid Films* **361**, 527 (2000).
- M. Burgelman, K. Decock, A. Niemegeers, J. Verschraegen, S. Degraeve, *Univ. Gent, Belgium* (2021).
- K. Kim, J.S. Yoo, S.K. Ahn, Y.J. Eo, J.S. Cho, J. Gwak, J.H. Yun, *Sol. Energy* **155**, 167 (2017).
- A. Shah, *Practical Handbook of Photovoltaics*, 209 (EPFL Press: 2012).
- T.K. Todorov, D.M. Bishop, Y.S. Lee, *Sol. Energy Mater. Sol. C.* **180**, 350 (2018).
- A. Srivastava, P. Dua, T.R. Lenka, S.K. Tripathy, *Mater. Today Proc.* **43**, 3735 (2020).
- A.D. Adewoyin, M.A. Olopade, M. Chendo, *Optik* **133**, 122 (2017).
- A.E.H. Benzetta, M. Abderrezek, M.E. Djeghlal, *Optik* **181**, 220 (2019).
- A.E. Benzetta, M. Abderrezek, M.E. Djeghlal, *J. Nano-Electron. Phys.* **10** No 5, 05035 (2018).
- S. Adachi, K. Ito, *Copp. Zinc Tin Sulfide-Based Thin-Film Sol. C.* **149** (2015).
- S. Chala, N. Sengouga, F. Yakuphanoglu, S. Rahmane, M. Bdirina, I. Karteri, *Energy* **164**, 871 (2018).
- J. Madan, Shivani, R. Pandey, R. Sharma, *Sol. Energy* **197**, 212 (2020).
- M. Elbar, S. Tobbeche, *Energy Procedia* **74**, 1220 (2015).
- A. Khanna, R. Pandey, J. Madan, A. Dhingra, *Opt. Mater.* **122**, 111677 (2021).
- A. Luque, S. Hegedus, *Handbook of Photovoltaic Science and Engineering* (John Wiley & Sons: 2011).
- J. Burdick, T. Glatfelter, *Sol. Cells* **18**, 301 (1986).
- S. Amiri, S. Dehghani, *J. Electron. Mater.* **49**, 5895 (2020).
- B. Bibi, B. Farhadi, A. Liu, *J. Comput. Electron.* **20**, 1769 (2021).

Моделювання тандемного сонячного елемента CZTS/CZTSe за допомогою програмного забезпечення SCAPS-1D

Leila Ghalmi¹, Souhila Bensmaine¹, Mourad Elbar², Slimane Chala^{2,3}, Hayat Merzouk¹

¹ *Materials and Renewable Energy Research Unit, Faculty of Sciences, Abou Bekr Belkaid University, 13000 Tlemcen, Algeria*

² *Laboratory of Metallic and Semiconducting Materials, Mohamed Khider University, 07000 Biskra, Algeria*

³ *Institute of Electrical and Electronic Engineering, M'Hamed Bougara University, 35000 Boumerdes, Algeria*

Сонячний спектр може бути розділений тандемними сонячними елементами на кілька субелементів, які мають різні ширини забороненої зони і ефективніше перетворюють світло в електрику, ніж окремі елементи. У роботі моделювання фотоелектричних (PV) характеристик тандемного сонячного елемента CZTS/CZTSe на основі структур сульфиду міді-цинку-олова (CZTS) як верхнього елемента та селеніду міді-цинку-олова (CZTSe) як нижнього елемента було виконано за допомогою симулятора SCAPS-1D при освітленні AM1.5. Спочатку було виконано моделювання окремих сонячних елементів CZTS і CZTSe і отримано ефективність відповідно 14,37 % і 17,87 %, що добре узгоджується з наявними результатами. До подачі відфільтрованого спектру змодельовані PV параметри тандемного сонячного елемента CZTS/CZTSe мають ефективність перетворення (η) 20,68 % і густину струму короткого замикання (J_{sc}) 20,205 мА/см² для верхнього та нижнього елементів з довільною нормальною товщиною. Крім того, щоб досягти узгодження струму, як верхній, так і нижній елементи були досліджені при різній товщині тандемної конфігурації, коли товщини верхнього та нижнього елементів були відповідно в діапазонах 0,05-0,5 мкм і 0,1-1 мкм. Продуктивність тандемного сонячного елемента визначалася після подачі відфільтрованого спектру та узгодження струму. Значення J_{sc} тандемного сонячного елемента CZTS/CZTSe становить 20,33 мА/см² для товщини 0,255 мкм верхнього, CZTS, елемента та товщини 0,8 мкм нижнього, CZTSe, елемента. Максимальний η , рівний 22,98 %, досягається для конструкції тандемної структури з підвищенням напруги холостого ходу (V_{oc}) на 1,48 В.

Ключові слова: Моделювання, SCAPS-1D, Тандемний сонячний елемент CZTS/CZTSe, Узгодження струму, Відфільтрований спектр.